PROGRESS IN COLOR, COLORANTS AND COATINGS

available online @ www.pccc.icrc.ac.ir

Progress in Color Colorants Coating 17 (2024), 159-173

Ministry of Science, Research and Technology
Institute for Color Science & Technology

The Photostabilizing Technology of Grapefruit Peel Extract on Polystyrene Thin Films: Concept Generation Using Morphological and Physical Properties

H. Ahmed[1], E. Yousif[*2], A. Ahmed[3], R. Yusop[4], K. Zainulabdeen[2], D.S. Ahmed[5], A. Rashad[2], A. Husain[3]

[1] Department of Chemistry, College of Science, Mustansiriyah University, P.O. Box 17022, Baghdad, Iraq
[2] Department of Chemistry, College of Science, Al-Nahrain University, P.O. Box 64021, Baghdad, Iraq
[3] Polymer Research Unit, College of Science, Mustansiriyah University, P.O. Box 17022, Baghdad, Iraq
[4] School of Chemical Sciences and Food Technology, Faculty of Science and Technology, Universiti Kebangsaan Malaysia, Bangi, P.O. Box 43600, Selangor, Malaysia
[5] Department of Chemical Industries, Institute of Technology-Baghdad, Middle Technical University, P.O. Box 10066, Baghdad, Iraq

ARTICLE INFO

Article history:
Received: 29 Sept 2023
Final Revised: 26 Oct 2023
Accepted: 28 Oct 2023
Available online: 20 Dec 2023

Keywords:
Grapefruits
Citrus peel
Photostabilizer
UV blocker
TINUVIN 622
Naringin

ABSTRACT

This paper discusses the effects of UV light exposure on Citrus paradisi (grapefruit) peel in terms of naringin and TINUVIN 622 (a commercial stabilizer) compounds. This study aimed to develop a plant extract with the necessary properties to protect polystyrene from sunlight. Polystyrene films containing a low concentration of naringin were prepared, and TINUVIN 622, a commercial UV light stabilizer, irradiated the polystyrene sheets for 300 hours. Following irradiation, the study examined the infrared spectrum of polystyrene, weight loss, molecular weight reduction, and changes in surface morphology. Naringin and TINUVIN 622 significantly reduced the photodegradation of polystyrene films, acting as photostabilizers when compared to blank films. Prog. Color Colorants Coat. 17 (2024), 159-173© Institute for Color Science and Technology.

1. Introduction

The concerns of people regarding their livelihood and health have escalated, leading to the increased popularity of natural health-promoting foods, with citrus fruits being one of the most frequently discussed items. Citrus fruits are abundant in nutrients, including vitamin C, carotenoids, and phenolic compounds, all of which contribute to their numerous beneficial qualities. These phytochemicals serve as antioxidants and may protect cells from the oxidative damage caused by free radicals [1, 2]. Many citrus varieties have long been employed in traditional Chinese medicine and are formally incorporated into the Chinese Pharmacopoeia, known as 'chenpi' [3]. Citrus fruits are renowned for their high levels of flavonoids, predominantly found in flavanone glycosides, such as narirutin, naringin, hesperidin, and neohesperidin [4]. Citrus peel, the primary by-product of citrus fruits, has garnered significant attention in research due to its rich content of biologically active compounds, including phenolic acids and flavonoids [5, 6]. The antioxidant properties and potential health benefits of phenolic acids have gained increased recognition and have been the subject of extensive investigation, particularly in chronic and degenerative diseases [7]. The skin serves as the primary defence barrier of the human body against harmful environ-

---

*Corresponding author: * emad_yousif@hotmail.com
https://doi.org/10.30509/pccc.2023.167205.1251

mental pollutants, various xenobiotics, and solar ultraviolet (UV) radiation. The solar UV spectrum consists of three sections: UVC (280 nm), UVB (280-320 nm), and UVA (320-400 nm) bands [8, 9]. The UVB portion represents approximately 5 % of the total solar UV radiation that reaches the Earth's surface. UVB radiation has been shown to suppress the immune system and also acts as a co-carcinogen, tumor initiator, and tumor promoter [10].

Exposure to UVB radiation is associated with a range of biological effects, including inflammation, the development of sunburn, changes in skin pigmentation, alterations in the immune system, and the induction of oxidative stress. These biological responses influence the development of various types of skin cancer [11, 12].

Basal cell carcinoma (BCC) and squamous cell carcinoma (SCC), collectively referred to as non-melanoma skin cancer, represent the most common types of cancer in humans, accounting for 80 % and 16 % of reported skin cancer cases, respectively [13]. The UVA range contains approximately 90-95 % of the remaining solar UV radiation. Longer wavelengths within the UVA spectrum enable deeper dermis penetration through the epidermis.

The adverse effects of UV radiation on human health, particularly its role in skin cancer development, cannot be overstated. As a result, it is imperative to develop effective photoprotective and chemopreventive strategies to mitigate this risk. Traditional approaches have used sunscreens, which incorporate a combination of cosmetic ingredients, physical blockers, and chemical absorbers.

The method has certain drawbacks, primarily related to the photo-instability of some chemical absorbers and the cutaneous absorption of physical blockers into more delicate tissues. On the other hand, it offers advantages, such as better penetration into labile tissues. In the case of chemical absorbers, the photoproducts of commonly used sunscreen agents remain unclear, and their effects are still subject to ongoing investigation.

Concerns about the size of particles in frequently used physical blockers, like titanium dioxide, have arisen, especially with nanoparticles that may penetrate deep into the dermis due to their small size (100 nm). Consequently, health regulatory authorities have established maximum allowable levels of these agents in various cosmetic products. Nonetheless, the desired level of protection and the sun protection factor (SPF) can significantly vary from one region to another [14].

This study aimed to develop a plant extract for use as a PS photostabilizer in sunscreen products, comprising a blend of plant extracts enriched with flavonoids. The study assessed the physicochemical stability, photostability, and surface morphology of naringin and TINUVIN 622 (a commercial stabilizer).

2. Experimental

2.1. Materials

Polystyrene (Mw = 250,000) was obtained from the Sigma-Aldrich Chemical Company (Gillingham, UK). Plant products: Fresh grapefruits (*Citrus Paradise*) were purchased from a local market in Baghdad, cleaned with distilled water, and divided into peel and edible parts. Grapefruit peel was dried in hot air at 40 °C for 48 h. The peels were taken out and pulverized using an electric blender to make small, homogeneous particles to increase the contact surface area between the polymeric chain and the solvent. Ground peels were directly subjected to the extraction process. Chemicals, solvents, and reagents were sourced from Merck (Gillingham, UK).

2.2. Methods

2.2.1. Instrumentation

A Jasco FT/IR-4200 spectrometer was used to conduct the Fourier Transform Infrared (FT-IR) spectra (4000-400 cm^{-1}) (Tokyo, Japan). Polystyrene films were irradiated at 25 °C, with a maximum wavelength of 365 nanometers and 6.43×10^{-9} $ein.dm^{-3}.s^{-1}$, using an accelerated weather-meter QUV tester that was purchased from Q-Panel Company located in Homestead, Florida, USA. The surface of Polystyrene films was examined using atomic force microscopy (AFM), utilizing a Veeco equipment (Plainview, NY, USA). The surface of the polystyrene was examined with a Scanning Electron Microscope (SEM) Inspect S50 (FEI Company, Czechia, Czech Republic) at an acceleration voltage of 15KV. Images of Polystyrene surface captured at a microscopic level using a Meiji Techno Microscope in Tokyo, Japan. The PS films were installed using 0.6 mm thick aluminium plate supports, and the thickness of the films (about 40 µm) was measured using a Digital Vernier Caliper 2610 A micrometre (Vogel GmbH, Kevelaer, Germany) (Q-Panel Company, Homestead, FL, USA).

2.2.2. Extraction process

As previously reported, 100 grams of ground peels were combined with 250 millilitres of 96 % ethanol in a Soxhlet apparatus (0.5 × 6 cm) and subjected to extraction for 30 minutes [15].

2.2.3. PS films preparation

PS (5 g) was stirred for 90 minutes at 25 °C in 100 mL of chloroform. A PS solution was mixed with natural extracts (0.025, 0.05, and 0.075 % by weight) and swirled for 30 minutes at 25 °C. The uniform liquid was poured into clean glass slides with a thickness of about 40 µm, and it was then dried for 24 hours at 25 °C.

2.2.4. Exposure to light

A UV Light (max = 365 nm and light intensity = 6.2 109 ein·dm^3.s^{-1} nm) was employed in a room-temperature accelerated weather-meter QUV tester (Philips, Saarbrücken, Germany) to irradiate the PS films. The PS films were rotated periodically to ensure the incident light intensity was consistent on both sides. Then, monitoring the changes in PS films by using different techniques: FT-IR Spectrophotometry, Weight Loss, Viscometry Method, Surface morphology: Optical microscope, Scanning electronic microscopy (SEM) and Atomic force microscopy (AFM).

3. Results and Discussion

In this study, the flavonoid glycoside known as naringin was successfully isolated. The isolation process involved extracting flavonoid compounds and obtaining pure naringin from grapefruit peel. This was achieved through preparative thin-layer chromatography and the Kolle method [16]. Naringin offers a range of additional and intriguing properties, including antioxidant capabilities, light-blocking effects, anti-inflammatory activities, and cost-effectiveness compared to other flavonoids like morin or catechin. Moreover, naringin has demonstrated broad-spectrum antimicrobial activity against various microorganisms, including bacteria such as *Escherichia coli*, *Staphylococcus aureus*, and *Listeria innocua*, as well as against different viruses and fungi [27].

Paper and thin-layer chromatography methods revealed retardation factor (Rf) values for four isolated compounds [17]. These values were compared with theoretical values obtained using various solvent systems as eluants. Naringin, while typically appearing pale yellow, is challenging to detect during chromatographic analysis unless chromogenic sprays are utilized. However, it's worth noting that naringin exhibits a yellow-green hue on paper when viewed under UV light, particularly with the assistance of ammonia vapor.

The color change to a deep yellow indicates the presence of natural flavonoid compounds. These flavonoid compounds were characterized using infrared analysis. The vibrational shift of the hydroxy group was observed in the IR spectrum as an absorption band at the wave number 3278 cm^{-1} (OH), further supported by the vibration of the −OH group at 1258 cm^{-1}. An absorption band at 2953 cm^{-1} corresponds to the C-H group of CH_3. Additionally, the presence of the C=C bond in the aromatic ring is indicated by an absorbance band at the wave number 1461 cm^{-1}.

The predominant part of the absorption band in the 1411 cm^{-1} wave number region is attributed to the C-H bond in CH_2, while the primary component in the 1378 cm^{-1} wave number area corresponds to the CH bond in CH_3. The C-O-C bonds in ether are represented by absorption bands at 1068 cm^{-1} and 1040 cm^{-1}. This infrared spectrum data shows the investigated molecule contains hydroxyl (-OH), an aromatic ring (C=C), CH_2, CH_3, and ether groups. Given the existence of these functional groups in the naringin structure, the structure of naringin, as shown in Figure 1, matches the results of the IR spectrum analysis, which further reinforces the identification of the isolated chemical as the naringin compound [18].

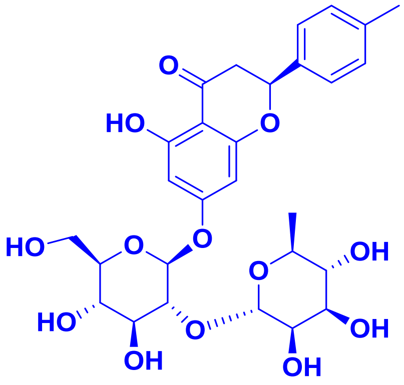

Figure 1: Structure of naringin [15].

3.1. FT-IR spectrophotometry

When PS is exposed to irradiation, polystyrene (PS) undergoes significant changes. It loses its mechanical properties, undergoes discoloration, and forms small polymeric fragments containing various functional groups [19, 20]. The presence of oxygen generates PS radicals, leading to the production of highly reactive oxygenated species. These species can react with hydrogen radicals, resulting in the formation of hydroxylated PS. The hydroxylated PS then further decomposes into hydroxyl radicals and oxygenated PS radicals, ultimately forming fragments containing carbonyl groups.

When PS blends are exposed to radiation, FTIR spectroscopy can be used to monitor the −C=O group, providing important information on the degree of photodegradation.

This study aimed to investigate the impact of naringin and TINUVIN 622 on the photodegradation of polystyrene (PS) using FTIR spectrometry [21]. The UV irradiation was applied individually to pure PS and PS blends for 300 hours, with samples collected for analysis at 50-hour intervals. The study focused on monitoring the intensity of the −C=O (1720 cm^{-1}) band compared to the unaffected −C−H band (ΔC-H) associated with the CH_2 groups that remained unaffected by the exposure to radiation [22]. Equation (1) was employed to calculate the increase in the -C=O group index (ΔC=O), which was subsequently represented as a function of the irradiation duration (Figure 3). The analysis involved the functional group ($As=A_{C=O}$) and the reference peak (Ar and A_{C-H}) (Eq. 1).

$$I_s=A_S/A_r \qquad (1)$$

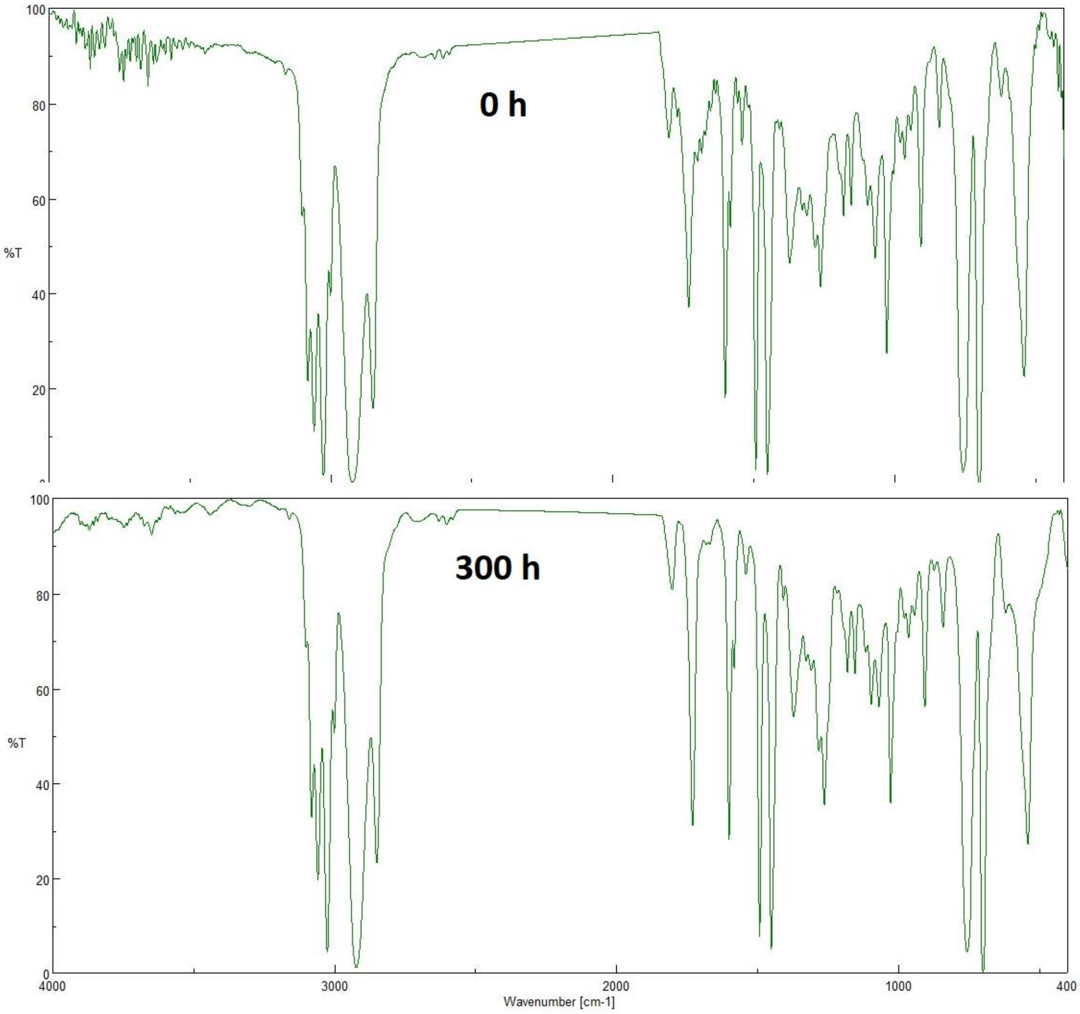

Figure 2: FTIR spectra of PS films before and after irradiation.

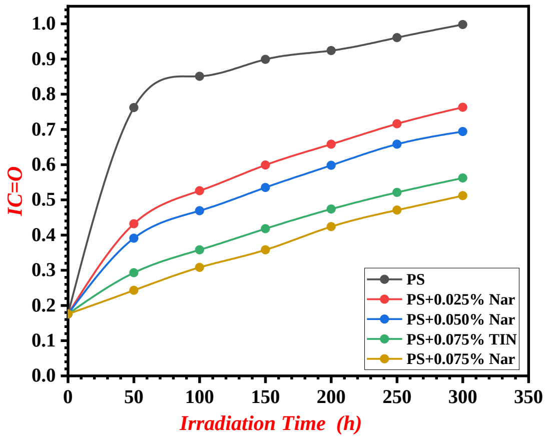

Figure 3: Effect of irradiation of PS films on carbonyl index.

3.2. PS films weight loss

Polystyrene soon changes from colourless to yellow when exposed to UV radiation at a high temperature for an extended period. It degrades due to small fragments and decreasing polymer weight [23].

UV light was projected on the PS films for up to 300 hours, and the weight loss was estimated using equation 2. The films were weighted before irradiation (W_1) and after irradiation at different times (W_2). The percentage of polymer weight loss resulting from irradiation was estimated via equation 2.

$$Weight\ loss\%= [(W_1-W_2)/W_1] \times 100 \tag{2}$$

The PS weight changed after 300 hours of radiation, as seen in Figure 4. The weight loss increased significantly after 50 hours until reaching 300 hours.

The blank PS film lost more polymer weight than PS, naringin, and TINUVIN 622 mixes with varied weight concentrations (0.025, 0.05, and 0.075 %). The least weight loss was seen with PS + 0.075 % naringen compared to the other plant extract concentrations.

3.3. Viscometry method

The Mark-Houwink equation was applied in this context, commonly used to determine the viscosity-average molecular weight (MV) for PS in solution [24]. Although this equation is suitable for various polymer ranges, it is not suitable for low molecular weight polymers. The anticipated decrease in PS viscosity with increasing irradiation time was attributed to the formation of crosslinks between polymeric strands [24]. The study aimed to investigate the impact of naringin and TINUVIN 622 (at concentrations of 0.025, 0.05, and 0.075 %) on MV variations in PS. The polymeric materials were exposed to radiation for 0 to 300 hours, and the subsequent MV changes were documented (Figure 5).

3.4. Microscopic surface morphology of PS films

Irradiating PS films induce defects and surface damage. The surface morphology of both the irradiated and non-irradiated PS films was analyzed using various microscopic techniques. Applying UV absorbers has been found to mitigate the photodegradation and photo-oxidation of polystyrene by absorbing harmful radiation [25]. The surface morphology of the PS (blank) film was observed under 400 × magnification before and after radiation exposure using a microscope (Figure 6).

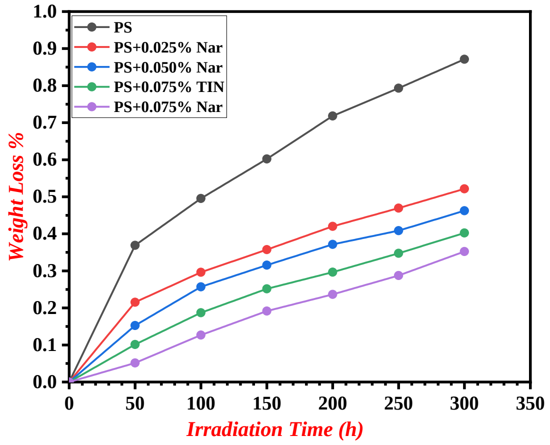

Figure 4: Effect of irradiation of PS films on weight loss (%).

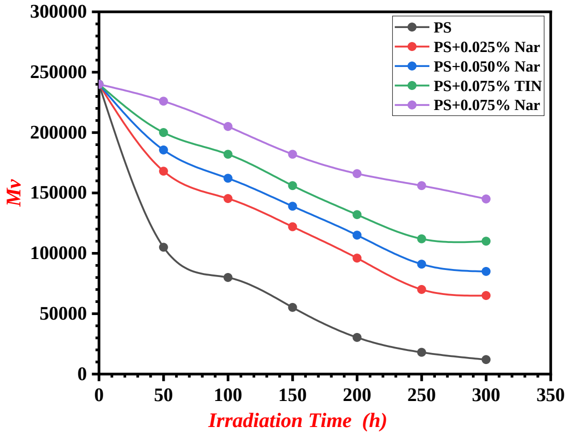

Figure 5: Alterations to the M_V of PS when exposed to radiation.

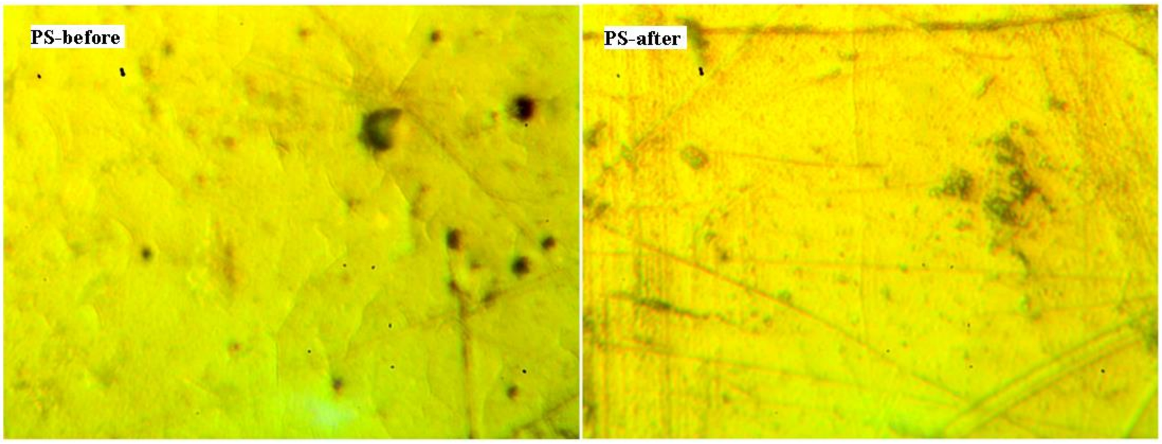

Figure 6: Microscopic pictures of PS and with various naringin and TINUVIN 622 blended concentrations both before and after irradiation.

The microscopic images of the non-irradiated films revealed a smooth surface, largely free of any significant white spots or furrows. Conversely, the microscopic images of the irradiated PS films exhibited uneven surfaces and various surface cracks. However, the additives resulted in fewer white spots and grooves than the PS film (blank), underscoring the effectiveness of naringin and TINUVIN 622 as photostabilizers for PS films (Figure 7).

3.5. PS scanning electron microscopy (SEM)

SEM is a powerful tool for exploring the surface morphology of polymers, providing insights into their internal structures [26]. Electron beams capture precise, magnified images of the PS surface. The SEM images of the non-irradiated PS films displayed a smooth, clean surface with well-defined grain boundaries and notable particle homogeneity (Figure 8).

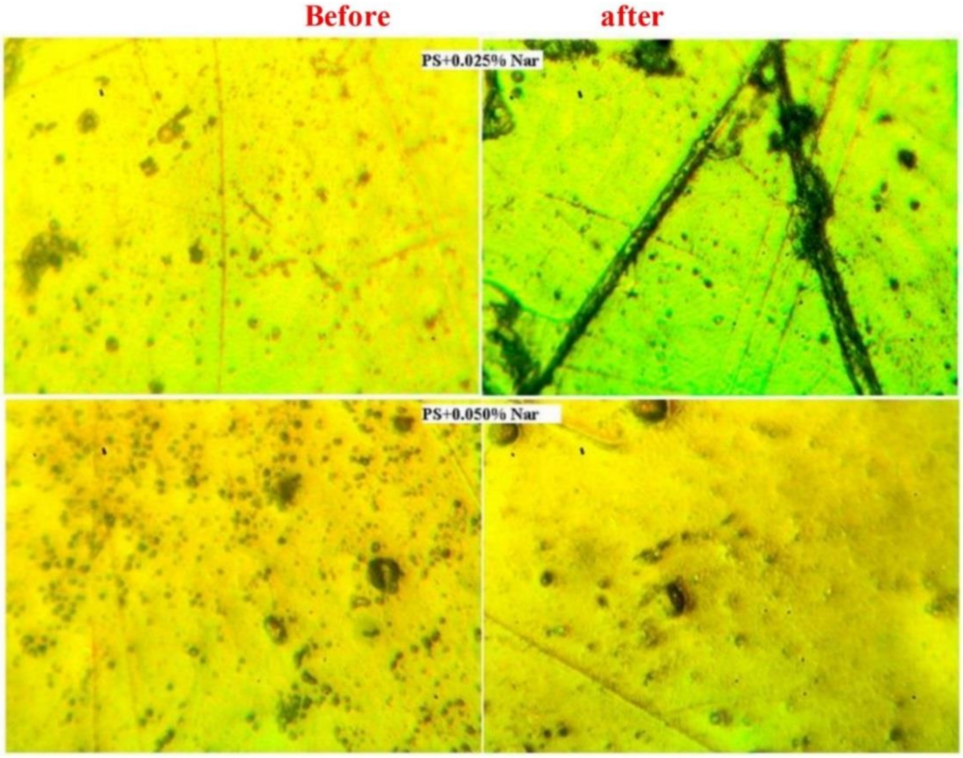

Figure 7: Microscopic images of PS and PS with different concentrations of naringin and TINUVIN 622 blends before and after irradiation.

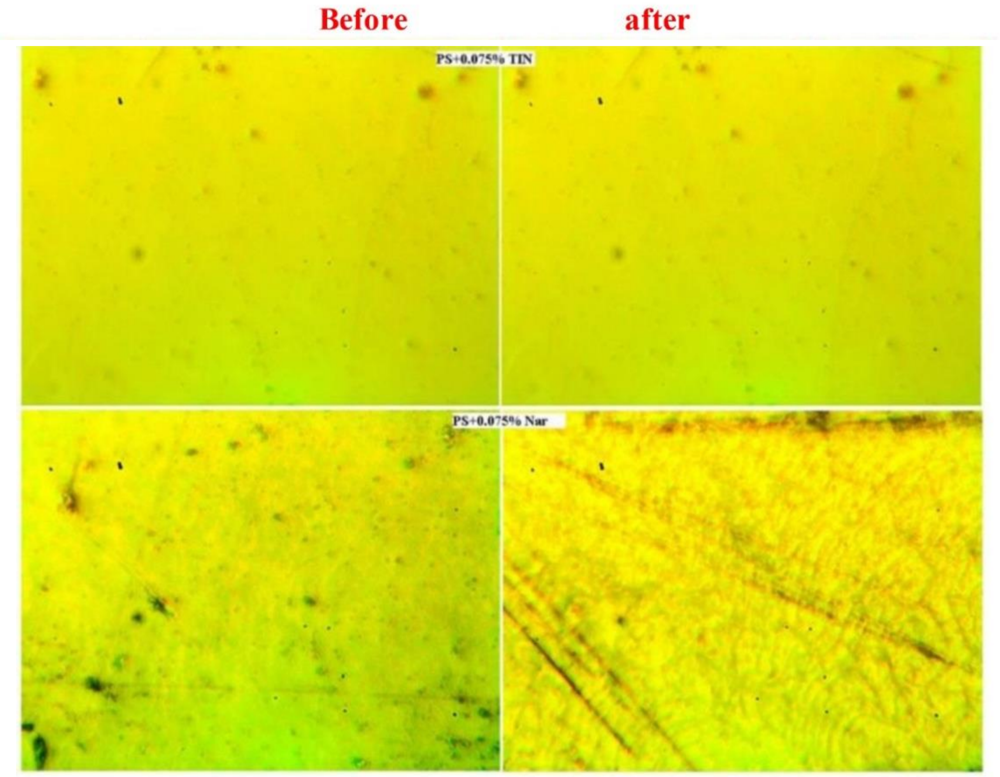

Figure 7: Continue.

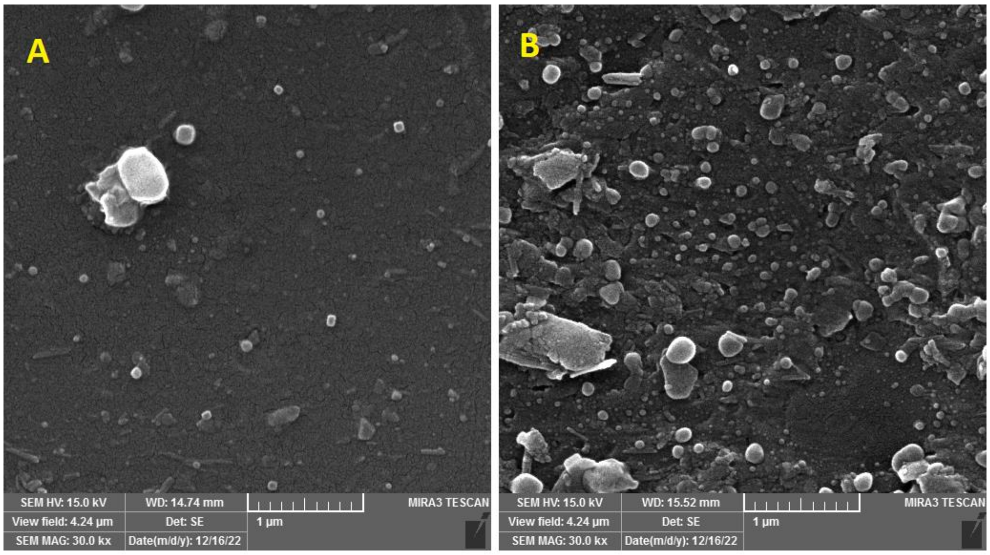

Figure 8: SEM images of PS (blank) (A) before and (B) after irradiation.

The introduction of naringin and TINUVIN 622 to the PS led to a notable change in particle size and their random distribution on the surface after 300 hours of UV irradiation. The SEM images of the PS films exhibited a visibly rough surface post-irradiation. It was evident that the surface morphology of the PS experienced significant changes following irradiation. Observations of PS with varying concentrations of plant extracts indicated that irradiation only minimally affected the dense texture (Figure 9). The notable resilience to irradiation observed in films with additives underscores the remarkable chemical stability of these blends.

3.6. PS atomic force microscopy (AFM)

The study of surface morphology and particle characteristics of materials can be effectively conducted using an AFM, a high-resolution scanning microscope [22, 24]. Accordingly, Figure 10 depicts the surface analysis of the PS films (surface area = 4.0× 4.0 m^2) before and after irradiation (Figure 10).

The PS films exhibited a smooth surface according to the two- and three-dimensional AFM scans. However, the blank PS film demonstrated a rough surface after exposure, indicating a high level of photodegradation. Compared to the blank PS film surface, the AFM images of the PS films containing additives revealed a significantly smoother and more uniform surface. Notably, PS+0.075 % Naringen showed more effective results in preventing PS photodegradation than other concentrations of naringin and commercial stabilizers. The PS film containing 1 demonstrated a highly homogeneous and smooth surface (Figure 11). The AFM images of the PS+0.075 % Naringen film showed a rough and featureless region. Specifically, the PS+0.025 % Nar, PS+0.05 % Nar, PS+0.075 % TIN, and PS+0.075 % Nar films exhibited surface roughness values of 342.7, 91.2, 78.5, 66.4, and 42.1 nm, respectively.

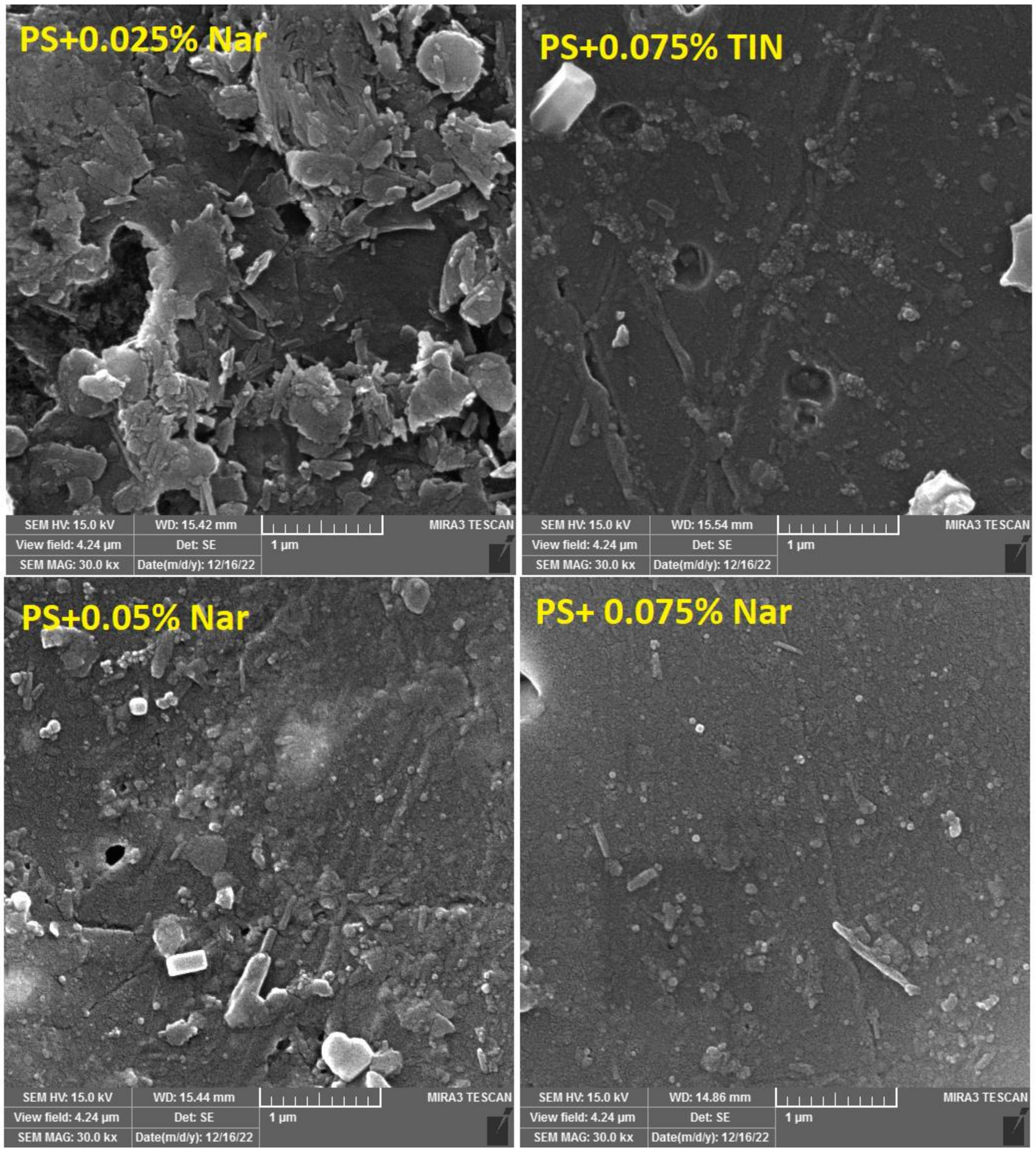

Figure 9: SEM images of PS and PS/ naringin and TINUVIN 622 before and after irradiation.

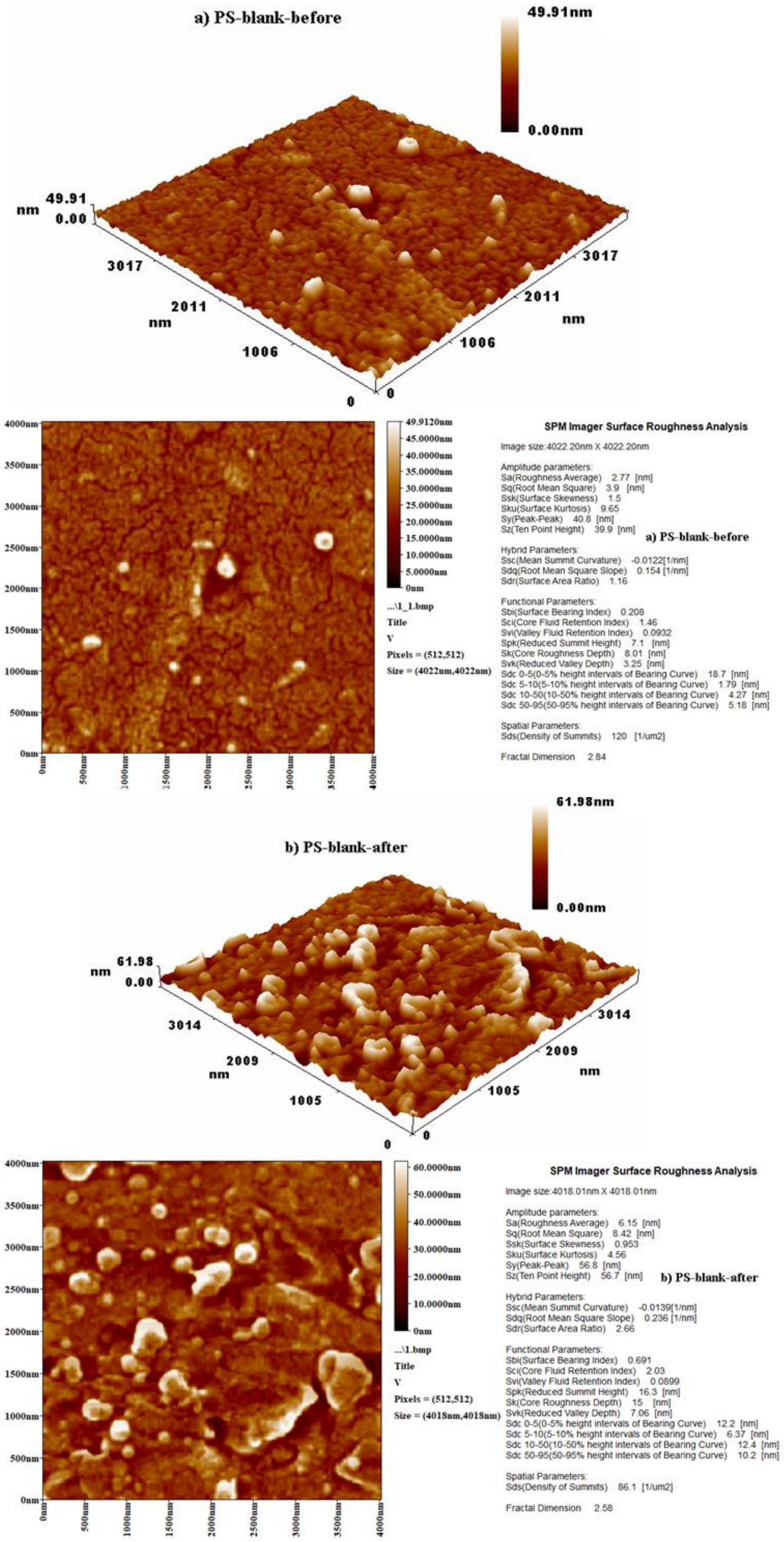

```
SPM Imager Surface Roughness Analysis

Image size:4022.20nm X 4022.20nm

Amplitude parameters:
Sa(Roughness Average)   2.77  [nm]
Sq(Root Mean Square)   3.9  [nm]
Ssk(Surface Skewness)   1.5
Sku(Surface Kurtosis)   9.65
Sy(Peak-Peak)   40.8  [nm]
Sz(Ten Point Height)   39.9  [nm]        a) PS-blank-before

Hybrid Parameters:
Ssc(Mean Summit Curvature)   -0.0122[1/nm]
Sdq(Root Mean Square Slope)   0.154 [1/nm]
Sdr(Surface Area Ratio)   1.16

Functional Parameters:
Sbi(Surface Bearing Index)   0.208
Sci(Core Fluid Retention Index)   1.46
Svi(Valley Fluid Retention Index)   0.0932
Spk(Reduced Summit Height)   7.1   [nm]
Sk(Core Roughness Depth)   8.01  [nm]
Svk(Reduced Valley Depth)   3.25  [nm]
Sdc 0-5(0-5% height intervals of Bearing Curve)   18.7  [nm]
Sdc 5-10(5-10% height intervals of Bearing Curve)   1.79  [nm]
Sdc 10-50(10-50% height intervals of Bearing Curve)   4.27  [nm]
Sdc 50-95(50-95% height intervals of Bearing Curve)   5.18  [nm]

Spatial Parameters:
Sds(Density of Summits)   120   [1/um2]

Fractal Dimension   2.84
```

```
SPM Imager Surface Roughness Analysis

Image size:4018.01nm X 4018.01nm

Amplitude parameters:
Sa(Roughness Average)   6.15  [nm]
Sq(Root Mean Square)   8.42  [nm]
Ssk(Surface Skewness)   0.953
Sku(Surface Kurtosis)   4.56
Sy(Peak-Peak)   56.8  [nm]
Sz(Ten Point Height)   56.7  [nm]        b) PS-blank-after

Hybrid Parameters:
Ssc(Mean Summit Curvature)   -0.0139[1/nm]
Sdq(Root Mean Square Slope)   0.236 [1/nm]
Sdr(Surface Area Ratio)   2.66

Functional Parameters:
Sbi(Surface Bearing Index)   0.691
Sci(Core Fluid Retention Index)   2.03
Svi(Valley Fluid Retention Index)   0.0899
Spk(Reduced Summit Height)   16.3  [nm]
Sk(Core Roughness Depth)   15    [nm]
Svk(Reduced Valley Depth)   7.06  [nm]
Sdc 0-5(0-5% height intervals of Bearing Curve)   12.2  [nm]
Sdc 5-10(5-10% height intervals of Bearing Curve)   6.37  [nm]
Sdc 10-50(10-50% height intervals of Bearing Curve)   12.4  [nm]
Sdc 50-95(50-95% height intervals of Bearing Curve)   10.2  [nm]

Spatial Parameters:
Sds(Density of Summits)   86.1  [1/um2]

Fractal Dimension   2.58
```

Figure 10: 2D and 3D AFM images of PS (blank) (a) before and (b) after irradiation.

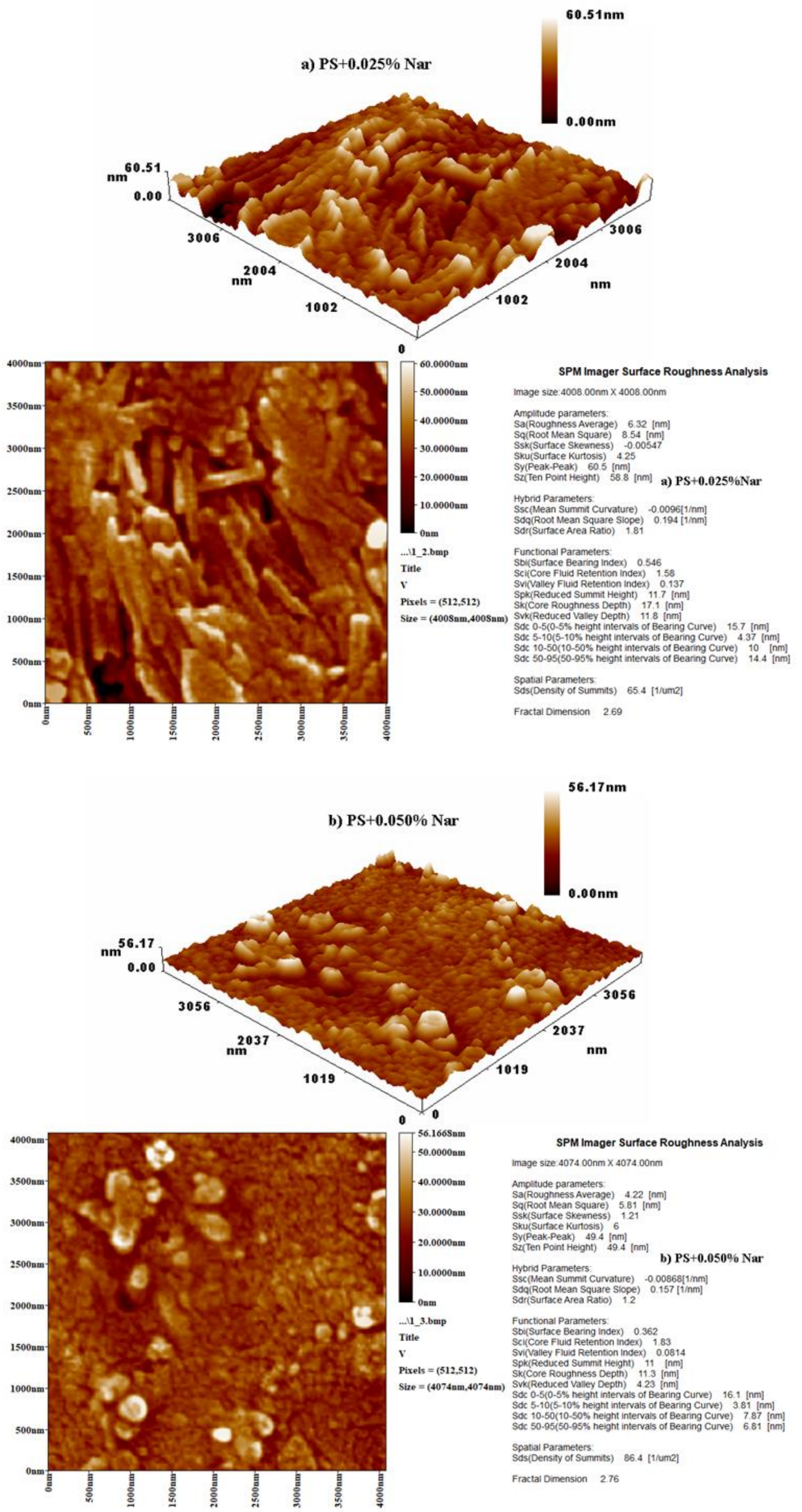

```
SPM Imager Surface Roughness Analysis

Image size:4008.00nm X 4008.00nm

Amplitude parameters:
Sa(Roughness Average)   6.32  [nm]
Sq(Root Mean Square)   8.54  [nm]
Ssk(Surface Skewness)   -0.00547
Sku(Surface Kurtosis)   4.25
Sy(Peak-Peak)   60.5  [nm]
Sz(Ten Point Height)   58.8  [nm]

Hybrid Parameters:
Ssc(Mean Summit Curvature)   -0.0096[1/nm]
Sdq(Root Mean Square Slope)   0.194 [1/nm]
Sdr(Surface Area Ratio)   1.81

Functional Parameters:
Sbi(Surface Bearing Index)   0.546
Sci(Core Fluid Retention Index)   1.58
Svi(Valley Fluid Retention Index)   0.137
Spk(Reduced Summit Height)   11.7  [nm]
Sk(Core Roughness Depth)   17.1  [nm]
Svk(Reduced Valley Depth)   11.8  [nm]
Sdc 0-5(0-5% height intervals of Bearing Curve)   15.7  [nm]
Sdc 5-10(5-10% height intervals of Bearing Curve)   4.37  [nm]
Sdc 10-50(10-50% height intervals of Bearing Curve)   10    [nm]
Sdc 50-95(50-95% height intervals of Bearing Curve)   14.4  [nm]

Spatial Parameters:
Sds(Density of Summits)   65.4  [1/um2]

Fractal Dimension   2.69
```

```
SPM Imager Surface Roughness Analysis

Image size:4074.00nm X 4074.00nm

Amplitude parameters:
Sa(Roughness Average)   4.22  [nm]
Sq(Root Mean Square)   5.81  [nm]
Ssk(Surface Skewness)   1.21
Sku(Surface Kurtosis)   6
Sy(Peak-Peak)   49.4  [nm]
Sz(Ten Point Height)   49.4  [nm]

Hybrid Parameters:
Ssc(Mean Summit Curvature)   -0.00868[1/nm]
Sdq(Root Mean Square Slope)   0.157 [1/nm]
Sdr(Surface Area Ratio)   1.2

Functional Parameters:
Sbi(Surface Bearing Index)   0.362
Sci(Core Fluid Retention Index)   1.83
Svi(Valley Fluid Retention Index)   0.0814
Spk(Reduced Summit Height)   11    [nm]
Sk(Core Roughness Depth)   11.3  [nm]
Svk(Reduced Valley Depth)   4.23  [nm]
Sdc 0-5(0-5% height intervals of Bearing Curve)   16.1  [nm]
Sdc 5-10(5-10% height intervals of Bearing Curve)   3.81  [nm]
Sdc 10-50(10-50% height intervals of Bearing Curve)   7.87  [nm]
Sdc 50-95(50-95% height intervals of Bearing Curve)   6.81  [nm]

Spatial Parameters:
Sds(Density of Summits)   86.4  [1/um2]

Fractal Dimension   2.76
```

Figure 11: 2D and 3D AFM images of (a) PS+0.025 % Nar, (b) PS+0.05 % Nar, (c) PS+0.075 % TIN, and (d) PS+0.075 % Nar films after irradiation.

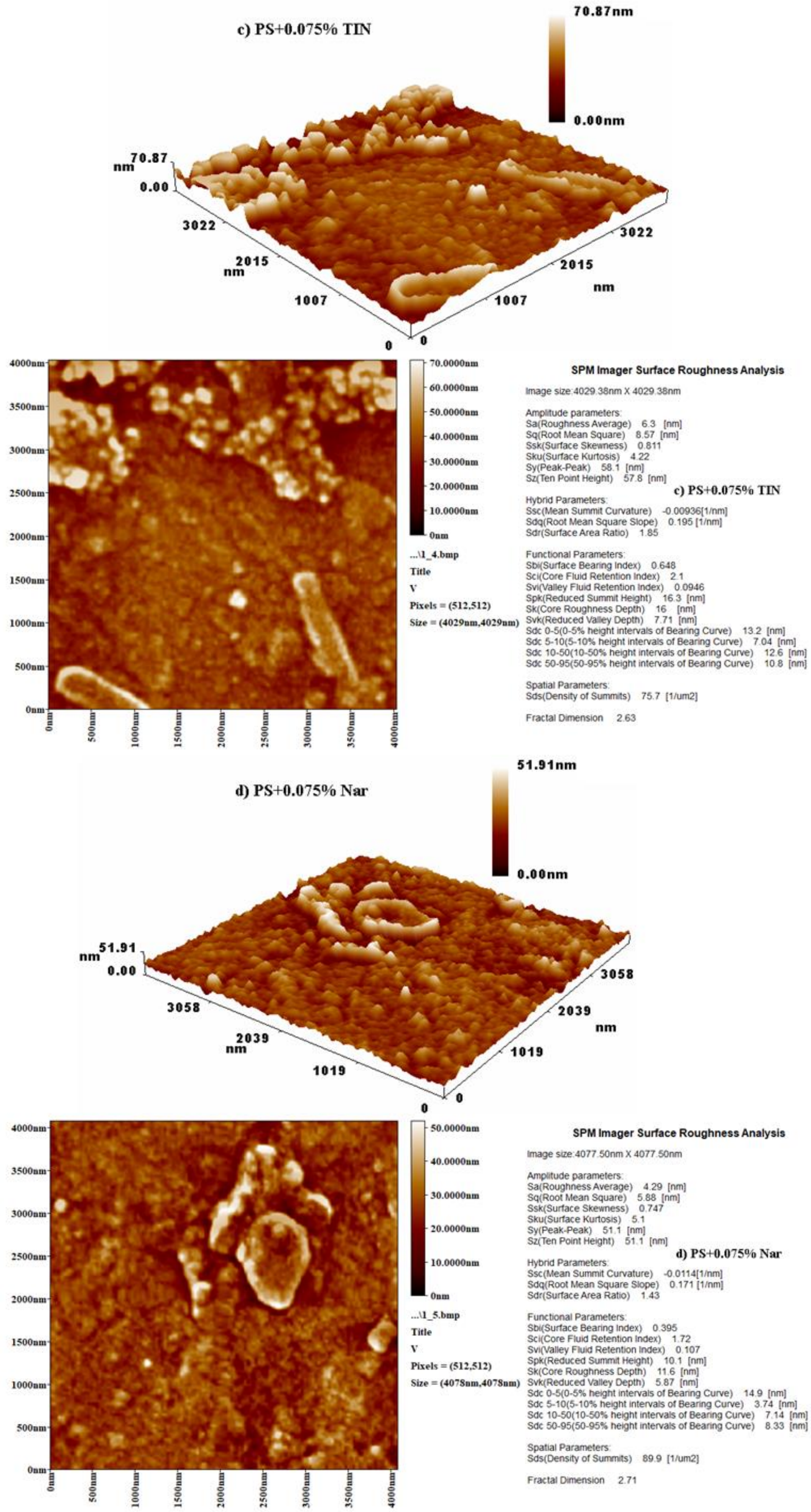

SPM Imager Surface Roughness Analysis

c) PS+0.075% TIN

Image size:4029.38nm X 4029.38nm

Amplitude parameters:
Sa(Roughness Average) 6.3 [nm]
Sq(Root Mean Square) 8.57 [nm]
Ssk(Surface Skewness) 0.811
Sku(Surface Kurtosis) 4.22
Sy(Peak-Peak) 58.1 [nm]
Sz(Ten Point Height) 57.8 [nm]

Hybrid Parameters:
Ssc(Mean Summit Curvature) -0.00936[1/nm]
Sdq(Root Mean Square Slope) 0.195 [1/nm]
Sdr(Surface Area Ratio) 1.85

Functional Parameters:
Sbi(Surface Bearing Index) 0.648
Sci(Core Fluid Retention Index) 2.1
Svi(Valley Fluid Retention Index) 0.0946
Spk(Reduced Summit Height) 16.3 [nm]
Sk(Core Roughness Depth) 16 [nm]
Svk(Reduced Valley Depth) 7.71 [nm]
Sdc 0-5(0-5% height intervals of Bearing Curve) 13.2 [nm]
Sdc 5-10(5-10% height intervals of Bearing Curve) 7.04 [nm]
Sdc 10-50(10-50% height intervals of Bearing Curve) 12.6 [nm]
Sdc 50-95(50-95% height intervals of Bearing Curve) 10.8 [nm]

Spatial Parameters:
Sds(Density of Summits) 75.7 [1/um2]

Fractal Dimension 2.63

SPM Imager Surface Roughness Analysis

d) PS+0.075% Nar

Image size:4077.50nm X 4077.50nm

Amplitude parameters:
Sa(Roughness Average) 4.29 [nm]
Sq(Root Mean Square) 5.88 [nm]
Ssk(Surface Skewness) 0.747
Sku(Surface Kurtosis) 5.1
Sy(Peak-Peak) 51.1 [nm]
Sz(Ten Point Height) 51.1 [nm]

Hybrid Parameters:
Ssc(Mean Summit Curvature) -0.0114[1/nm]
Sdq(Root Mean Square Slope) 0.171 [1/nm]
Sdr(Surface Area Ratio) 1.43

Functional Parameters:
Sbi(Surface Bearing Index) 0.395
Sci(Core Fluid Retention Index) 1.72
Svi(Valley Fluid Retention Index) 0.107
Spk(Reduced Summit Height) 10.1 [nm]
Sk(Core Roughness Depth) 11.6 [nm]
Svk(Reduced Valley Depth) 5.87 [nm]
Sdc 0-5(0-5% height intervals of Bearing Curve) 14.9 [nm]
Sdc 5-10(5-10% height intervals of Bearing Curve) 3.74 [nm]
Sdc 10-50(10-50% height intervals of Bearing Curve) 7.14 [nm]
Sdc 50-95(50-95% height intervals of Bearing Curve) 8.33 [nm]

Spatial Parameters:
Sds(Density of Summits) 89.9 [1/um2]

Fractal Dimension 2.71

Figure 11: Continue.

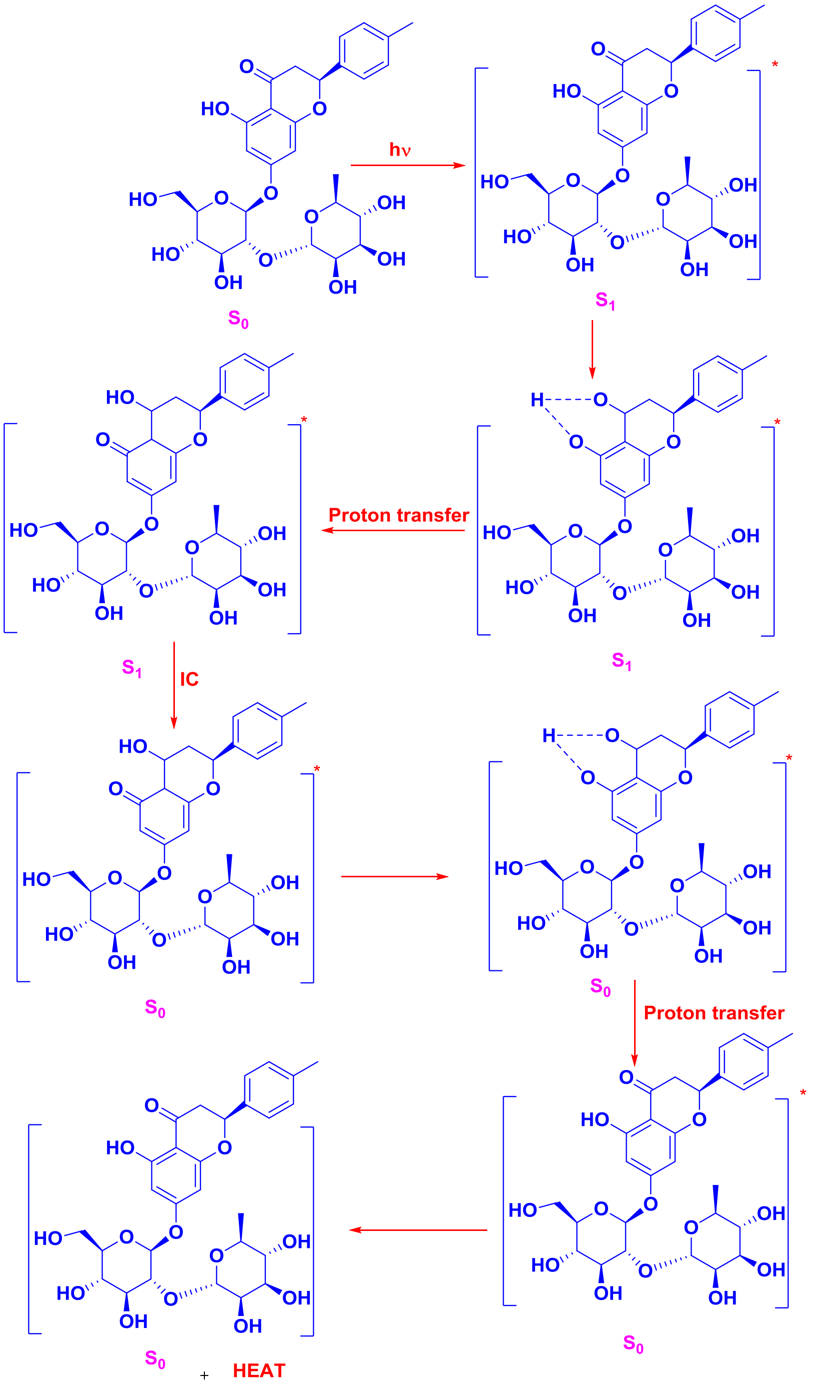

Scheme 1: The suggested mechanism of photostabilization of II is through UV light absorption and light energy dissipation as heat.

3.7. Suggested mechanisms of photostabilization of PS

UV-Vis and IR spectroscopy results were employed to propose a mechanism for the impact of additives on PS films after radiation. The additive was a blend of flavonoids, including naringin, studied as a single material. The commonly accepted mechanisms for additives in photostabilization encompass UV absorption (screening), free radical scavenging (chain-breaking donors), and excited state quenching (physical quenching). Based on these mechanisms, we propose Scheme 1 for the absorption of UV light by naringin and its conversion into heat energy, thereby protecting the PS films from direct photo-excitation.

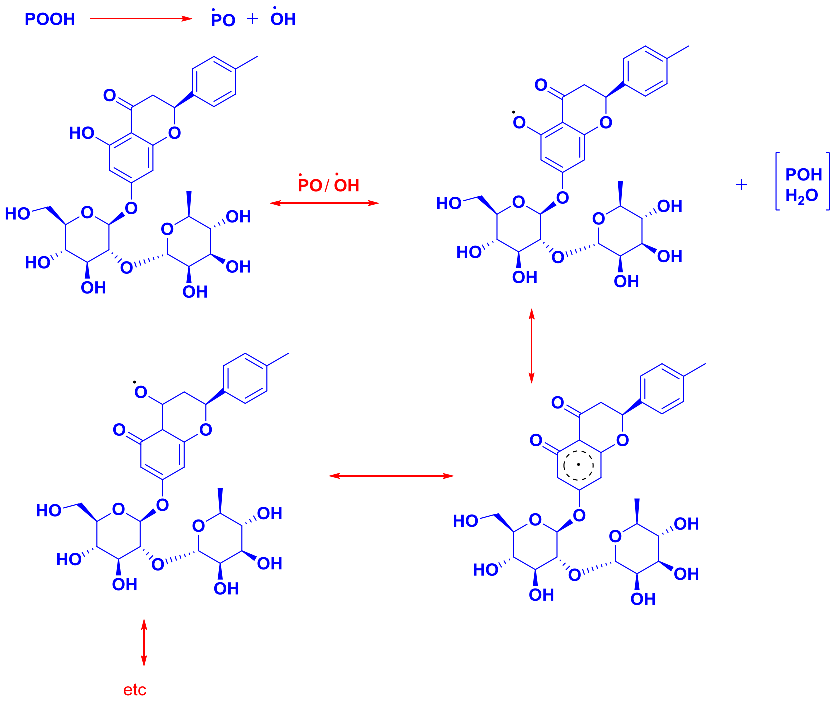

Scheme 2: The suggested mechanism of photostabilization as a radical scavenger.

It is also understood that β-substituted hydroxybenzophenones or benzotriazoles can function as radical scavengers (chain-breaking donors) during photostabilization. Therefore, in addition to its role as a UV absorber, naringin demonstrates the potential to act as an additive with radical scavenging properties, serving as a chain-breaking donor, as illustrated in Scheme 2.

Naringin can undergo tautomerism, converting from flavonone to 2-hydroxy chalcone, which may explain its effectiveness as a photostabilizer, achieved through either UV absorption or the free radical scavenging mechanism. Enol transforms into a trans-keto form under the influence of UV light irradiation. However, the trans-keto form reverts to the enol form through thermal back-isomerization or exposure to visible light [22]. Coumarin and its derivatives have been extensively studied owing to their highly efficient dimerization and cleavage reactions, which occur without the need for photosensitizers or catalysts, as well as their exceptional biological activities, biocompatibility, and adjustable fluorescent properties. Under 365 nm light irradiation, coumarins dimerize to form a cyclobutane ring through [2 + 2] cycloaddition, which can be cleaved under 254 nm light irradiation, leading to the restoration of the original structure via a photoemission reaction. Incorporating coumarin units into the gel matrix should allow for the reversible formation of additional crosslinks, facilitating the spatial tuning of the network structure [28].

4. Conclusions

Various concentrations (0.025, 0.05, and 0.075 %) of naringin were efficiently extracted using a simple procedure alongside TINUVIN 622 as a commercial stabilizer. The isolated plant extract (naringin) was characterized using infrared spectroscopy and thin-layer chromatography. To assess their influence on the photostability of polymeric blends, naringin and TINUVIN 622 were incorporated into polystyrene. As anticipated, upon exposure to ultraviolet light, both naringin and TINUVIN 622 substantially reduced the photodegradation of the material. Several analytical techniques, such as infrared spectroscopy, weight loss analysis, molecular weight reduction evaluation, and surface alterations in polystyrene, were used to explore how naringin and TINUVIN 622 stabilize polystyrene. Notably, PS+0.075 % naringin exhibited the most significant stabilizing effect compared to other concentrations.

5. References

1. Kris-Etherton PM, Hecker KD, Bonanome A Coval SM, Binkoski AE, Hilpert KF, Griel AE, et al. Bioactive compounds in foods: their role in the prevention of cardiovascular disease and cancer. Am. J. Med.2002;113(9)(Suppl. 2):71-88. https://doi.org/ 10.1016/S0002-9343(01)00995-0
2. Silalahi J. Anticancer and health protective properties of citrus fruit components. Asia Pacific journal of clinical nutrition. 2002; 11(1):79-84. https://doi.org/ 10.1046/j.1440-6047.2002.00271.x
3. Pharmacopoeia of People's Republic of China 2000 (in Chinese); Chemical Industry Press: Beijing, China, 2000; pp 108-108.
4. Rouseff RL, Martin SF, Youtsey CO. Quantitative survey of narirutin, naringin, hesperidin, and neohesperidin in citrus. J Agri Food Chem. 1987; 35(6):1027-30. https://doi. org/10.1021/jf00078a040
5. Bocco A, Cuvelier ME, Richard H, Berset C. Antioxidant activity and phenolic composition of citrus peel and seed extracts. J Agri Food Chem. 1998; 46(6):2123-9. https://doi. org/10.1021/jf9709562
6. Manthey JA, Grohmann K. Phenols in citrus peel byproducts. Concentrations of hydroxycinnamates and polymethoxylated flavones in citrus peel molasses. J Agri Food Chem.. 2001; 49(7):3268-73. https://doi. org/ 10.1021/jf010011r
7. Lodovici M, Guglielmi F, Meoni M, Dolara P. Effect of natural phenolic acids on DNA oxidation in vitro. Food Chem Toxi. 2001; 39(12):1205-10. https://doi. org/10.1016/S0278-6915(01)00067-9
8. Baliga MS, Katiyar SK. Chemoprevention of photocarcinogenesis by selected dietary botanicals. Photochem Photobiol Sci. 2006;5(2):243-53. https://doi.org/10.1039/B505311K
9. Sklar LR, Almutawa F, Lim HW, Hamzavi I. Effects of ultraviolet radiation, visible light, and infrared radiation on erythema and pigmentation: a review. Photochem Photobiol Sci. 2012; 12:54-64. https://doi. org/10.1039/c2pp25152c.
10. Katiyar SK. Grape seed proanthocyanidines and skin cancer prevention: inhibition of oxidative stress and protection of immune system. Mol Nutri Food Res. 2008; 52(S1):S71-6. https://doi.org/ 10.1002/mnfr. 200700198
11. Hruza LL, Pentland AP. Mechanisms of UV-induced inflammation. J Invest Dermatol. 1993; 100(1):S35-41. https://doi.org/10.1038/jid.1993.21.
12. Krause M, Klit A, Blomberg Jensen M, Søeborg T, Frederiksen H, Schlumpf M, et al. Sunscreens: are they beneficial for health? An overview of endocrine disrupting properties of UV-filters. Inter J And. 2012 Jun;35(3):424-36.https://doi.org/10.1111/j.1365-2605. 2012.01280.x
13. Bowden GT. Prevention of non-melanoma skin cancer by targeting ultraviolet-B-light signalling. Nature Rev Cancer. 2004; 4(1):23-35. https://doi. org/10.1038/nrc1253
14. Maier H, Schauberger G, Martincigh BS, Brunnhofer K, Hönigsmann H. Ultraviolet protective performance of photoprotective lipsticks: change of spectral transmittance because of ultraviolet exposure. Photoderm Photoimmunol Photomed. 2005; 21(2):84-92. https://doi.org/10.1111/j.1600-0781.2005.00143.x
15. Ahmed H, Ahmed A, Yousif E, Ahmed DS, Kadhom M, Husain A, et al. Effect of ecofriendly grapefruit peel extract on PVC thin films photostabilizing tested under harmful weathering conditions. J Vinyl Add Technol. https://doi.org/10.1002/vnl.22029
16. Gentili B, Horowtiz RM. Chromatography of dihydrochalcone sweeteners and related compounds: A reagent for detecting dihydrochalcones. J Chromatograph A. 1971; 63:467-9. https://doi.org/ 10. 1016/S0021-9673(01)85678-8
17. Shriner RL, Hermann CK, Morrill TC, Curtin DY, Fuson RC. The systematic identification of organic compounds. John Wiley & Sons; 2003 Aug 19.
18. Hakim A, Loka IN, Prastiwi NW. New method for isolation of naringin compound from Citrus maxima. Natural Res. 2019; 10(08):299. 10.4236/nr.2019. 108019
19. Biazar E, Zeinali R, Montazeri N, Pourshamsian K, Behrouz MJ, Asefnejad A, et al. Cell engineering: nanometric grafting of poly-N-isopropylacrylamide onto polystyrene film by different doses of gamma radiation. Intern J Nanomed. 2010:549-56. https://doi.org/10.2147/IJN.S8269
20. Sharma T, Aggarwal S, Kumar S, Mittal V, Kalsi PC, Manchanda VK. Effect of gamma irradiation on the optical properties of CR-39 polymer. J Mater Sci. 2007; 42:1127-30. https://doi.org/10.1007/s10853-006-0516-7
21. Kiatkamjornwong S, Sonsuk M, Wittayapichet S, Prasassarakich P, Vejjanukroh PC. Degradation of styrene-g-cassava starch filled polystyrene plastics. Poly Degradation Stability. 1999; 66(3):323-35. https://doi.org/10.1016/S0141-3910(99)00082-8
22. Yousif E, Ahmed DS, El-Hiti GA, Alotaibi MH, Hashim H, Hameed AS, et al. Fabrication of novel ball-like polystyrene films containing Schiff base microspheres as photostabilizers. Polymers. 2018; 10(11):1185.. https://doi.org/10.3390/polym10111185
23. Ahmed A, Abdallh M, Al-Mashhadani MH, Ahmed DS, Bufaroosha M, Jawad AH, et al. Environmental stability of poly (vinyl chloride) modified by schiff's base under exposure to UV. Biointerface Res Appl Chem. 2021; 11(5):13465-73. https://doi.org/10. 33263/ BRIAC115.1346513473
24. Yaseen AA, Yousif E, Al-Tikrity ET, El-Hiti GA, Kariuki BM, Ahmed DS, et al. FTIR, weight, and surface morphology of poly (vinyl chloride) doped with tin complexes containing aromatic and heterocyclic moieties. Polymers. 2021; 13(19):3264. https://doi.org/10.3390/polym13193264
25. Ahmed AA, Al-mashhadani MH, Hashim H, Ahmed DS, Yousif E. Morphological, color impact and

spectroscopic studies of new schiff base derived from 1, 2, 4-triazole ring. Prog Color Colorant Coat. 2021; 14(1):27-34. 10.30509/PCCC.2021.81664

26. Arraq RR, Hadi AG, Ahmed DS, Al-Mashhadani MH, Hashim H, Ahmed AA, et al. Color Changes, AFM and SEM Study of PVC/triorganotin (IV)-Cephalexin Complexes Samples Via UV Radiation. Prog Color Colorant Coat. 2023; 16(3):283-94. 10.30509/PCCC.2023.167075.1195
27. Guzman-Puyol S, Hierrezuelo J, Benítez JJ, Tedeschi G, Porras-Vázquez JM, Heredia A, et al. Transparent, UV-blocking, and high barrier cellulose-based bioplastics with naringin as active food packaging materials. Inter J Biol Macromol. 2022; 209:1985-94. https://doi.org/10.1016/j.ijbiomac.2022.04.177
28. Zhu CN, Li CY, Wang H, Hong W, Huang F, Zheng Q, et al. Reconstructable gradient structures and reprogrammable 3D deformations of hydrogels with coumarin units as the photolabile crosslinks. Adv Mater. 2022; 33(18):2008057. https://doi.org/10.1002/adma.202008057.

How to cite this article:
Ahmed H, Yousif E, Ahmed A, Yusop R, Zainulabdeen K, Ahmed DS, Rashad A, Husain A. The Photostabilizing Technology of Grapefruit Peel Extract on Polystyrene Thin Films: Concept Generation Using Morphological and Physical Properties. Prog Color Colorants Coat. 2024;17(2):159-173. https://doi.org/10.30509/pccc.2023.167205.1251.